

A search for active galactic nuclei in the most extreme UV-selected starbursts using the European VLBI Network

R. Alexandroff,^{1*} R. A. Overzier,² Zsolt Paragi,^{3,4} Antara Basu-Zych,⁵ Tim Heckman,⁶ Guinevere Kauffmann,⁷ Stephen Bourke,³ Andrei Lobanov,⁸ Andy Ptak⁵ and David Schiminovich⁹

¹*Department of Astrophysical Sciences, Princeton University, Peyton Hall-Ivy Lane, Princeton, NJ 08544, USA*

²*Department of Astronomy, University of Texas at Austin, C1400, 1 University Station, Austin, TX 78712, USA*

³*Joint Institute for VLBI in Europe (JIVE), Postbus 2, 7990 AA Dwingeloo, the Netherlands*

⁴*MTA Research Group for Physical Geodesy and Geodynamics, PO Box 91, H-1521 Budapest, Hungary*

⁵*Goddard Space Flight Center, Greenbelt, MD 20771, USA*

⁶*Center for Astrophysical Sciences, Department of Physics and Astronomy, Johns Hopkins University, Baltimore, MD 21218, USA*

⁷*Max Planck Institute for Astrophysics, D-85748 Garching, Germany*

⁸*Max-Planck-Institut für Radioastronomie, D-53121 Bonn, Germany*

⁹*Department of Astronomy, Columbia University, New York, NY 10027, USA*

Accepted 2012 March 19. Received 2012 February 20; in original form 2011 October 19

ABSTRACT

We have used the European very long baseline interferometry (VLBI) Network (EVN) to observe a sample of Lyman break analogues (LBAs), nearby ($z < 0.3$) galaxies with properties similar to the more distant Lyman break galaxies (LBGs). The study of LBGs may help define the feedback relationship between black holes (BHs) and their host galaxies. Previous Very Large Array (VLA) observations have shown that the kpc-scale radio emission from LBAs is dominated by starbursts. The main targets of this VLBI experiment were selected because they possessed emission-line properties between starbursts and Type 2 (obscured) active galactic nuclei (AGN). Eight targets (three star-forming LBAs, four composite LBAs and one Type 1 AGN) were observed at 5 GHz, four of which (one star-forming LBA and three composite LBAs) were also observed at 1.7 GHz. One star-forming LBA and one composite LBA were detected above 5σ at 1.7 GHz (only), while the AGN was detected at 5 GHz. In both LBAs, the radio luminosity (L_R) exceeds that expected from supernovae (remnants) based on a comparison with Arp 220, Arp 229A and Mrk 273, by factors of 2–8. The composite LBA exhibits a compact core emitting around 10 per cent of the VLA flux density. The high T_b of 3.5×10^7 K and excess core L_R with respect to the L_R/L_X relation of radio-quiet AGN indicate that this LBA possesses an obscured AGN ($M_{\text{BH}} \sim 10^{5-7} M_{\odot}$). In three other composite LBAs detected previously in the X-ray, no radio sources were detected, indicating either variability or the presence of an obscured AGN below our radio sensitivity. While weak AGN may coexist with the starbursts as shown in at least one of the LBAs, their contribution to the total radio flux is fairly minimal. Our results show that the detection of such weak AGN presents a challenge at radio, X-ray and optical emission-line wavelengths at $z \sim 0.2$, indicating the great difficulties that need to be overcome in order to study similar processes at high redshift when these types of galaxies were common.

Key words: techniques: interferometric – galaxies: active – galaxies: ISM – galaxies: starburst – radio continuum: galaxies.

1 INTRODUCTION

The nuclei of local galaxies contain supermassive black holes (BH). Evidence suggests that these BHs have grown over time following the mass increase of their host galaxies in accordance with the $M_{\text{BH}}-\sigma$ or $M_{\text{BH}}-M_{\text{bulge}}$ relations (Magorrian et al. 1998; Gebhardt

*E-mail: rmalexan@princeton.edu

et al. 2000). Furthermore, feedback between these BHs and their hosts is an essential element of structure formation models as it has been proposed that they regulate or suppress star formation as a result of active galactic nucleus (AGN) activity (e.g. Di Matteo, Springel & Hernquist 2005). One must thus approach Galaxy formation with both star formation and BH accretion in mind.

Starburst galaxies at high redshift, such as the ultraviolet (UV) selected Lyman break galaxies (LBGs) or their dusty counterparts such as the sub-millimetre galaxies (SMGs), are the precursors of present-day massive galaxies undergoing a phase of intense star formation (e.g. Adelberger et al. 2005). A significant fraction of their stellar mass is contained in large, dense stellar clumps. It has been suggested that these giant clumps could host seed BHs that merge in the centre of the galaxy (Elmegreen, Bournaud & Elmegreen 2008), where they can continue to grow further through other accretion events. It has been shown that the majority of SMGs at high redshift host an AGN as indicated by their X-ray emission (Alexander et al. 2005), while the fraction among LBGs is a few per cent at most (Steidel et al. 2002; Lehmer et al. 2005; Laird et al. 2006; Ouchi et al. 2008; Zheng et al. 2010). One possible explanation for this discrepancy is a delay expected between the moment of onset of the starburst and the moment that a galaxy is able to feed its BH, as one has to wait for the strong winds and supernovae (SNe) from the most massive stars to have ceased before gas can fall on to the BH (Norman & Scoville 1988; Davies et al. 2007). This would be consistent with the relatively young ages of typical LBGs at $z \simeq 3\text{--}4$ compared to the dustier and more evolved SMGs.

Although the majority of LBGs do not appear to host luminous AGN, it is difficult to detect the presence of a low-luminosity AGN (LLAGN), especially when it is at the centre of a powerful starburst. From studies in the local Universe we know that weak or absent X-ray emission does not necessarily imply that an accreting BH is absent. LLAGN have a large range in optical-to-X-ray luminosity ratios, and many are very weak in hard X-rays due to heavy obscuration (Heckman et al. 2005b). Other AGN identification techniques, such as the commonly used diagnostic tests based on optical emission line ratios (e.g. Baldwin, Phillips & Terlevich 1981, ‘BPT’ diagrams), can also yield inconclusive results. These line ratios are susceptible to, e.g., dust, metallicity, age and star formation history (Kewley et al. 2006; Yuan, Kewley & Sanders 2010). New low-velocity shock models furthermore show that the line ratios arising in purely star-forming or starbursting environments are often indistinguishable from those that are due to a combination of star formation and some AGN contributions, both occupying the same ‘composite’ region of the BPT diagram (Rich, Kewley & Dopita 2011). These problems can be partly alleviated by disentangling the emission from different galaxy components (e.g. nucleus versus outer parts) using integral field spectroscopy, but this is currently not feasible at high redshifts except for the most extended galaxies.

We previously selected a rare population of nearby ($z < 0.3$) galaxies that are remarkably similar to LBGs in most of their basic physical properties. These ‘Lyman break analogues’ (LBAs) are similar to LBGs in mass, age, size, metallicity, optical extinction, star formation rate (SFR) and gas velocity dispersion (Heckman et al. 2005a; Hoopes et al. 2007). They also have morphologies similar to those at $z = 2\text{--}4$ (Overzier et al. 2008, 2010), and have similar emission-line kinematics (Basu-Zych et al. 2009; Gonçalves et al. 2010) and a similar interstellar medium dominated by strong feedback from massive, clumpy starburst regions (Overzier et al. 2009; Heckman et al. 2011). While none of the sources shows any evidence for an unobscured (Type 1) AGN (largely by selection), it is

unclear whether some may host obscured (Type 2) LLAGN. A small subset of LBAs falls in the composite region of the BPT diagram. These sources were also found to have the densest and most massive nuclei reminiscent of extremely young bulges (Overzier et al. 2009). An obvious question to ask is whether we see any evidence for BH growth.

At low intrinsic radio luminosities, the total radio emission of AGN is often dominated by the star formation in their host galaxies (e.g. Kimball et al. 2011; Padovani et al. 2011). High-resolution very long baseline interferometry (VLBI) observations can be used to search for the elusive LLAGN through their compact, high brightness temperature radio emission amidst other compact sources corresponding to radio supernovae (RSNe) and supernova remnants (SNRs) frequently seen on pc scales by allowing us to identify excess radio emission above that expected for RSN and SNR models (Kewley et al. 2000; Bondi et al. 2005; Gallimore et al. 2006; Biggs, Younger & Ivison 2010; Perez-Torres et al. 2010). Previous VLBI surveys have primarily targeted dusty galaxies [e.g. luminous infrared galaxies (LIRGs) or ultraluminous infrared galaxies (ULIRGs)] in the nearby universe (e.g. Corbett et al. 2003; Parra et al. 2010). The UV-selected LBA sample allows us to study the relationship between nuclear starbursts and BHs in an environment more similar to that expected at high redshift. We present the results from a pilot project using the European VLBI Network (EVN) exploring for the first time the compact radio structures in the nuclei of LBAs. The structure of this paper is as follows. In Section 2 we present our sample and give details on the 6 and 18 cm radio observations and data reduction methods. In Section 3 we present the main results. We discuss the implications of our results in Section 4, and conclude with a summary in Section 5. Throughout this paper, we assume a cosmology $[\Omega_M, \Omega_\Lambda, H_0] = [0.27, 0.73, 73.0]$ (with H_0 in $\text{km s}^{-1} \text{Mpc}^{-1}$) so that the angular scales at $z = 0.1, 0.2$ and 0.3 are $\approx 1.8, 3.2$ and 4.3 pc mas^{-1} .

2 SAMPLE, OBSERVATIONS AND DATA REDUCTION

For this experiment we targeted LBAs that were previously detected at the $\gtrsim 0.5 \text{ mJy}$ level in the Very Large Array (VLA) observations of Basu-Zych et al. (2007). Our VLBI sub-sample consists of three sources that are unlikely to host an AGN, and four sources that may be of starburst–AGN composite type based on their optical emission line ratios (Overzier et al. 2009). For comparison, we also include an eighth source showing strong evidence for pure AGN emission. We note that this source has similar far-UV (FUV) properties as the LBAs but it does not satisfy the full LBA selection criteria because the latter were designed to exclude pure AGN. Details on the sources are given in Table 1.

Two separate sets of observations were completed using the EVN over the course of two years. EVN observations of J0150+1308, J0213+1259, J0921+4509 and J2103–0728 were carried out at 1.7 GHz on three days between 2008 June 4 and 8. The participating telescopes were the Lovell Telescope in Jodrell Bank, the 14-element Westerbork Synthesis Radio Telescope, Effelsberg, Onsala (25 m), Medicina, Noto, Torun, Urumqi, Shanghai and Cambridge. Baselines therefore ranged from 198 to 8476 km. The aggregate bit rate per telescope was 1024 Mbps using 2-bit sampling and 4 s integration time. There were $8 \times 16 \text{ MHz}$ subbands each with 32 channels in both left-circular polarization (LCP) and right-circular polarization (RCP).

To extend the coherence time, the targets were phase-referenced to nearby calibrators with separations of $0^\circ\text{--}2^\circ$ selected from the

Table 1. Basic source parameters of our sample. The coordinates are from SDSS. The 1.4-GHz VLA flux densities and radio SFRs are from Basu-Zych et al. (2007). Optical line ratios are from Overzier et al. (2009), L_{FIR} and $\text{SFR}(\text{UV}+\text{IR})$ are from Overzier et al. (2011), and 2–10 keV X-ray luminosities are from Jia et al. (2011). The radio-derived SFRs agree very well with those based on the UV+IR, indicating that the radio emission is dominated by star formation.

α (J2000) (h m s)	δ (J2000) ($^{\circ}$ $'$ $''$)	z	$\frac{[\text{O III}]}{[\text{H}\beta]}$	$\frac{[\text{N III}]}{[\text{H}\alpha]}$	Type	$S_{1.4}^{\text{VLA}}$ (mJy)	$\text{SFR}_{1.4}$ ($M_{\odot} \text{ yr}^{-1}$)	$\text{SFR}_{\text{UV}+\text{IR}}$ ($M_{\odot} \text{ yr}^{-1}$)	$\log L_{\text{FIR}}$ (L_{\odot})	$\log L_X$ (erg s^{-1})
01:50:28.42	+13:08:58.1	0.147	2.29	0.21	SF-LBA	1.50	30.9	57.1	11.40	–
08:15:23.39	+50:04:14.6	0.164	0.76	0.29	SF-LBA	0.67	17.7	–	–	–
13:53:55.90	+66:48:00.5	0.198	1.74	0.16	SF-LBA	0.57	22.5	26.8	11.05	–
02:13:48.54	+12:59:51.4	0.219	0.78	0.81	COMP-LBA	0.90	44.3	56.1	11.38	41.63
08:08:44.26	+39:48:52.3	0.091	0.58	0.66	COMP-LBA	<0.5	<6	11.5	10.47	41.60
09:21:59.39	+45:09:12.4	0.235	0.74	0.50	COMP-LBA	1.41	81.5	87.1	11.57	42.36
21:03:58.73	–07:28:02.2	0.137	0.93	0.76	COMP-LBA	3.84	68.1	62.4	11.36	41.68
10:29:59.95	+48:29:37.9	0.232	4.17	0.45	AGN	0.85	–	–	–	–

Very Long Baseline Array (VLBA) Calibrator List.¹ The calibrator positions were accurate to within 0.20–1.32 mas. Within the phase-reference cycle of about 8 min, 100 s was spent on calibrators and 280 s on the targets, and there were 30 s gaps included for system temperature measurements. The total on-source time per target was about 3.5 h, which would ideally lead to a thermal noise below $10 \mu\text{Jy beam}^{-1}$.

Follow-up EVN observations of an extended sample, now including J0808+3948, J0815+5004, J1029+4829 and J1353+6648, were carried out at 5 GHz on 2010 March 19–20 (see Table 1). A higher frequency was used in this second run because it was believed to lead to higher detection rates: the expected flat spectrum emission from an AGN core would dominate over the steep spectrum emission from star-forming regions and it was expected that free-free absorption would not play a dominant role at this frequency. The array included the Lovell Telescope, Yebes (40 m), Westerbork, Effelsberg, Onsala (25 m), Medicina, Noto and Torun. The resulting baselines ranged from 266 to 2279 km. The data were recorded at 1024 Mbps in a similar fashion to the first observations (2-bit sampling and a 2 s integration time). There were 8×16 MHz subbands each with 32 channels in both LCP and RCP polarizations. Targets were again phase-referenced to calibrators with angular separations of 0.5 – 2° . A phase-reference cycle of 90–300 s on the calibrators and targets, respectively, was employed. The total on-source time on the targets was between 1 and 2 h. The expected rms noise was below $\sim 15 \mu\text{Jy beam}^{-1}$ allowing for $>5\sigma$ detections for targets at the level of $100 \mu\text{Jy}$.

The data were correlated by the EVN Data Processor at the Joint Institute for VLBI in Europe (JIVE). For data reduction and analysis we used the National Radio Astronomy Observatory (NRAO) Astronomical Image Processing System (AIPS). We followed standard data reduction procedures (e.g. Diamond 1995): the data were amplitude calibrated with measured gain curves and system temperatures then fringe-fitted and bandpass calibrated using the compact calibrator sources. Anomalous solutions were manually flagged in AIPS using the task SNEDT to view calculated rate and delay solutions. Subband 8 for the Lovell telescope and subband 7 for Torun were completely flagged in the second set of observations using task UVFLG due to poor bandpass solutions. The calibrated target data were averaged in time and frequency and then exported to UVFITS format. Additional manual flagging was carried out in DIFMAP (Shepherd, Pearson & Taylor 1994). For the second set of data collected on

2010 March, amplitude calibration was verified on several compact calibration sources (J0209+1352, J0808+4950 and J1344+6606) in DIFMAP. The sources were cleaned using repeated calls to CLEAN and SELFAL and then the amplitude corrections were examined using GSCALE. It was noted that across all calibrator sources all Torun amplitudes were off by a factor of 1.7, while Noto subband 7 amplitudes were off by a factor of 1.5 and subband 8 amplitudes were off by a factor of 1.7. Systematic corrections were made to these subbands using the AIPS task CLCOR and then the data was re-exported to UVFITS format. Possible sources of such systematic errors include faulty T_{sys} measurements due to RFI usually present across most subbands.

Dirty maps were formed with natural weighting (uvw 0, -2) using the MAPPLOT command in DIFMAP. For each target source the peak brightness and rms noise were determined. The results are listed in Table 2. For the two safe detections we show clean maps in Fig. 1.

3 RESULTS

For the 1.7 GHz data two sources, J0150+1308 (star-forming LBA) and J0921+4509 (composite LBA), were detected above 5σ . J0150+1308 is located at $(\alpha, \delta)_{\text{J2000}}$ of (01:50:28.39531, +13:08:58.0833). J0921+4509 is located at (09:21:59.40425, +45:09:12.4232). Both have a positional error of approximately 1 mas. For the 5.0 GHz data only one source was detected above 5σ , J1029+4829 (the AGN), while the two sources detected at 1.7 GHz were not. J1029+4829 is located at (10:29:59.95930, +48:29:38.0012) with a positional error of approximately 2 mas. Real detections should exhibit the synthesized beam pattern in their images due to the beam pattern's large effect on the noise in any image, although this cannot be seen at very low signal-to-noise ratios (S/N values). The two LBAs detected at 1.7 GHz exhibit this beam pattern in their dirty images suggesting that they are safe detections. The strong detection of these two sources at 1.7 GHz demonstrates the success of our phase-referencing efforts. We believe that the sources that remained undetected at 1.7 GHz are diffuse radio sources which lack a compact core detectable on the scale of our observations. Applying a uv -taper to downweight longer baselines, testing the effects of possibly over-resolving the flux, did not lead to a detection thus strengthening our reasoning that these are indeed faint sources.

At 5 GHz one likely detection just above 5σ was made. For the source J1029+4829 (AGN) the peak brightness location did not

¹ <http://www.vlba.nrao.edu/astro/calib/index.shtml>

Table 2. Measured value of rms noise, peak brightness and signal-to-noise ratio of the peaks for our eight targets (four targets were observed both at 1.658 and 4.990 GHz). Upper limits are given for non-detections. Note that because both observations used a different array configuration and the *L*-band run included Chinese and South African telescopes, the resolution from the two runs was quite similar.

Source	ν (GHz)	Noise ($\mu\text{Jy beam}^{-1}$)	Peak ($\mu\text{Jy beam}^{-1}$)	S/N	Beam (mas)	T_b (10^5K)
J0150+1308	1.658	15	149	9.9	8.6×6.2	>32.0
J0213+1259	1.658	14	<54	<3.9	5.9×7.8	<5.0
J0921+4509	1.658	15	113	7.5	5.7×15.9	>1.1
J2103-0728	1.658	17	<73	<4.3	6.3×10.2	<5.4
J0150+1308	4.990	26	<111	<4.3	6.1×8.5	<1.1
J0213+1259	4.990	26	<115	<4.4	6.1×8.7	<1.2
J0808+3948	4.990	35	<162	<4.6	5.2×10.1	<1.7
J0815+5004	4.990	31	<117	<3.8	5.1×9.3	<1.1
J0921+4509	4.990	25	<100	<4.0	5.4×8.1	<1.1
J1029+4829	4.990	24	127	5.3	7.1×9.4	>1.2
J1353+6648	4.990	25	<98	<3.9	5.5×8.3	<1.0
J2103-0728	4.990	27	<111	<4.1	7.1×10.2	<0.8

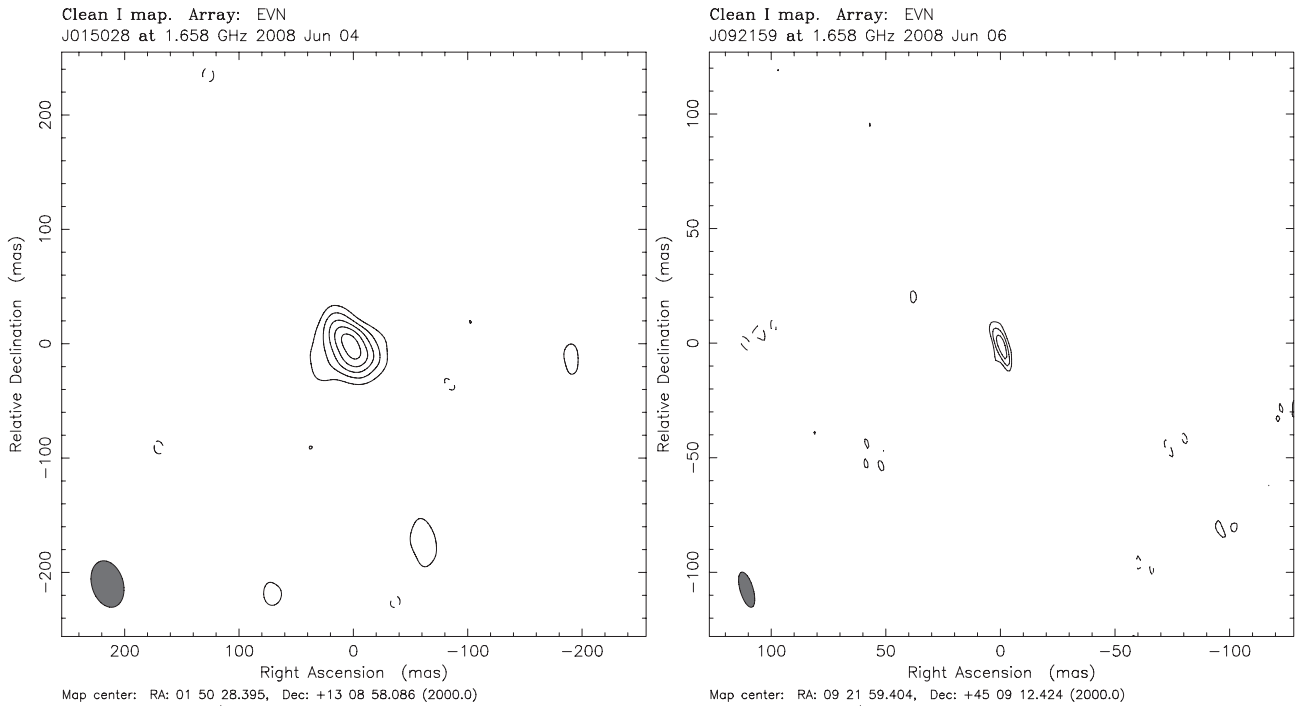


Figure 1. Naturally weighted clean maps of J0150+1308 (left) and J0921+4509 (right) at 1.7 GHz. The data for J0150+1308 were additionally weighted with a Gaussian taper of 0.5 at a uv -distance of $10 \text{ M}\lambda$. The contour levels are $\pm 1, 1.5, 2, 2.5$ and 3 times the 3σ noise of $45 \mu\text{Jy beam}^{-1}$, the tapered beam is $41.7 \times 27.5 \text{ mas}$ at PA $16^\circ 8'$, and the peak brightness is $148 \mu\text{Jy beam}^{-1}$. In the case of J0921+4509 the contour levels are $\pm 1, 1.5$ and 2 times the 3σ noise of $45 \mu\text{Jy beam}^{-1}$, the beam is $15.9 \times 5.7 \text{ mas}$ at PA $16^\circ 3'$, and the peak brightness is $111 \mu\text{Jy beam}^{-1}$.

vary when applying a strong uv -taper or when removing baselines or observation times suggesting a probable detection. Observations with a greater sensitivity would be needed to confirm this detection. The two sources detected at 1.7 GHz were not detected at 5 GHz. This result could be explained in several possible ways. One option is that our phase-referencing did not work well. Alternatively, the sources did not have compact emission well exceeding the $100 \mu\text{Jy}$ level so the sources were completely resolved in this observation. Finally, it is possible that they had spectra of ($\alpha \leq -0.1, S \propto \nu^\alpha$) calculated using the 5σ upper limit.

For the detected sources, parameters were obtained by fitting point and/or circular Gaussian model components to the uv -data using the MODELFIT command in DIFMAP. The results are summarized in Table 3. It should be noted that in all cases less than 50 per cent of the measured VLA flux density was recovered. For the source J0150+1308 (star-forming) only an extended model significantly larger than the restoring beam produced a good fit. Fitting a point-source model on the map left residual emission on the dirty map, indicating a more extended structure. Thus the non-detection of J0150+1308 (star-forming) at 5 GHz is most likely due to

Table 3. Modelfit results and brightness temperatures for all detections near or above 5σ . J0150+1308 (star-forming) could be fitted well only by a circular Gaussian model but J0921+4509 (composite) gave similarly good results when fitted by a point source, a compact circular Gaussian smaller than the beam and a more extended model. Here we give the compact circular Gaussian model size (see text). For the weakest detection, J1029+4829 (AGN), only a point model was used. In this case the geometric average of the beam major and minor axes is given as the upper limit for the size.

Source	ν (GHz)	S (μ Jy)	Ratio (EVN/VLA)	r (mas)	T_b (10^6 K)
J0150+1308	1.658	456	0.304	59.3	0.10
J0921+4509	1.658	111	0.079	1.32	34.9
J1029+4829	4.990	126	N/A	<9.4	>0.12

over-resolution. On the other hand, J0921+4509 (composite) could be fit equally well with a point source, a relatively compact circular Gaussian (~ 1.32 mas), or a more extended Gaussian source model (with size about the same as the major axis of the restoring beam).

Brightness temperatures were determined for each source detected using the formula

$$T_{b,\text{vlbi}} = 1.22 \times 10^{12} (1+z) \frac{S}{\theta_1 \theta_2 \nu^2}, \quad (1)$$

where S is the flux density (Jy), θ_1 and θ_2 are the major and minor axes of the fitted Gaussian model component [mas or full width at half-maximum (FWHM) for a point source] and ν is the observing frequency (GHz).

Because we could not distinguish between point and extended models in the case of J0921+4509 (composite), we used a Monte Carlo simulation of 1000 trials to attempt to constrain the source size. All Monte Carlo simulations were carried out using PARSELTONGUE (Kettenis et al. 2006) to call the relevant AIPS task repeatedly. Taking the 1.7 GHz field of J0213+1259 (composite) as a non-detection field we used the AIPS task UVSUB to add a point source directly to the uv -data. Random noise was simulated by placing the source at a different location in the field with every call to UVSUB. The AIPS task OMFIT was then used to fit a circular Gaussian model to this point source. Trials were conducted with initial modelfit parameters of both 2 and 10 mas for the major axis and giving the correct location of the simulated source. In both cases, the results were strongly peaked at a size of 0 mas, though an initial fit parameter of 10 mas occasionally led OMFIT to give results between 10 and 15 mas as the estimation of the size of our point source. We repeated the trials adding phase errors of 10 rms by using PARSELTONGUE to manually edit the SN table of our data set. When fitting a 10 mas model to these data the secondary peak between 10 and 15 mas was more pronounced. So while one of our modelfit results for J0921+4509 had a radius of up to 15.9 mas, our simulations reveal that the radio source could still be unresolved with a much smaller radius, especially given expected phase errors in our data.

Next we performed a similar trial but attempted to fit a Gaussian model to an inserted Gaussian source of 10 mas. The initial model provided to OMFIT exactly matched the simulated source. While results of the modelfit program tended to cluster around 10 mas, there was a spread of ± 5 mas with and without phase errors of 10 rms. Thus any modelfit result obtained is likely accurate to within ± 5 mas. However, this trial never produced results in the region of 1 mas. In our simulations an extended model comparable to the beam size can be fit by a weak point source accurately, but it is not possible to fit well an extended source with a compact model much

smaller than the beam. Since the VLBI structure of J0921+4509 (composite) can be fit well with compact models, it is most likely that the true size of the source is about 1.32 mas, with an error of ± 5 mas.

To summarize, we conclude that we have made two safe detections, one of which, J0150+1308 (star-forming), was resolved at 59.3 mas while the other, J0921+4509 (composite), is practically unresolved at 1.32 mas. In the next section we will discuss the interpretation of these results.

4 DISCUSSION

4.1 Pre-existing evidence for hidden AGN in composite LBAs

In order to address the question of whether weak AGN are present in the nuclear starburst regions of the LBAs, we specifically targeted four LBAs having optical emission-line spectra intermediate between pure starbursts and Type 2 AGN (J0213+1259, J0808+3948, J0921+4509 and J2103-0728). We also targeted three objects that, at least according to their main optical emission line ratios, are not suspected of having an obscured AGN present (J0150+1308, J0815+5004 and J1353+6648), and one source that is an AGN (J1029+4829). These sources are shown in the optical emission-line diagnostics diagram in Fig. 2 (BPT diagram).

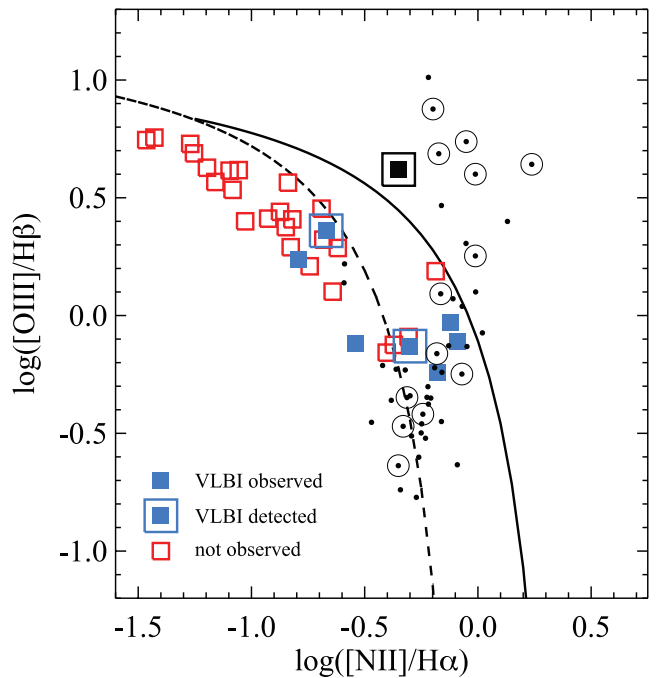


Figure 2. Optical emission-line diagnostic diagram according to Baldwin et al. (1981, BPT). The LBA sample studied in Overzier et al. (2009) is indicated by red/blue squares. Filled, blue squares mark LBAs that have been observed as part of our VLBI campaign, while (open) red squares mark LBAs that were not observed with VLBI. Objects detected during our EVN experiment are marked by the large, open blue squares. The black filled square indicates the AGN-like object J1029+4829 that was observed as part of this sample but is not an LBA. Small dots indicate LIRGs from the northern COLA sample from Parra et al. (2010) also observed with VLBI, with detections marked by the large open circles. Objects that lie in the region of the diagram in between the dotted and dashed lines are so-called starburst-AGN composite objects, while objects to the left of the dashed line and to the right of the solid line are H II-like and AGN-like objects, respectively (Kauffmann et al. 2003; Kewley et al. 2006).

Previous work has shown that the LBAs that lie in the composite part of the BPT diagram have a number of other properties as well that make them peculiar with respect to the ‘non-composite’ LBAs: Overzier et al. (2009) showed that they are host to particularly dense and compact starbursts (radii of the order of 100 pc), reaching stellar mass densities comparable to those of dense star clusters, while being up to 1000 times more massive (stellar masses of $\approx 10^8$ – $10^9 M_\odot$). They also tend to be the most massive galaxies in the LBA sample, and have the highest SFR (several tens to a hundred $M_\odot \text{ yr}^{-1}$, the exception being J0808+3948). Heckman et al. (2011) presented FUV spectra obtained with *Hubble Space Telescope* (*HST*)/Cosmic Origins Spectrograph (COS) that showed that these dense, compact starburst regions drive powerful winds with median and maximum velocities several times higher than that seen in typical starbursts, including LBGs at high redshift. Based on the starburst nature of the FUV spectra, the high wind speeds and the lack of evidence of unobscured (i.e. Type 1) AGN, it was argued that these are momentum-driven winds caused by the intense SN activity in the compact starbursts at the base of the wind. Finally, Jia et al. (2011) found the first plausible evidence for the presence of low-luminosity, obscured AGN in some or all of six composite LBAs observed in the X-ray. The presence of an AGN was inferred from elevated levels (factors of 2–10) of hard X-ray emission over that expected from the SFR– L_X sequence formed by pure star-forming galaxies (see Fig. 3). However, the SFR– L_X correlation and its scatter are not particularly well constrained, making

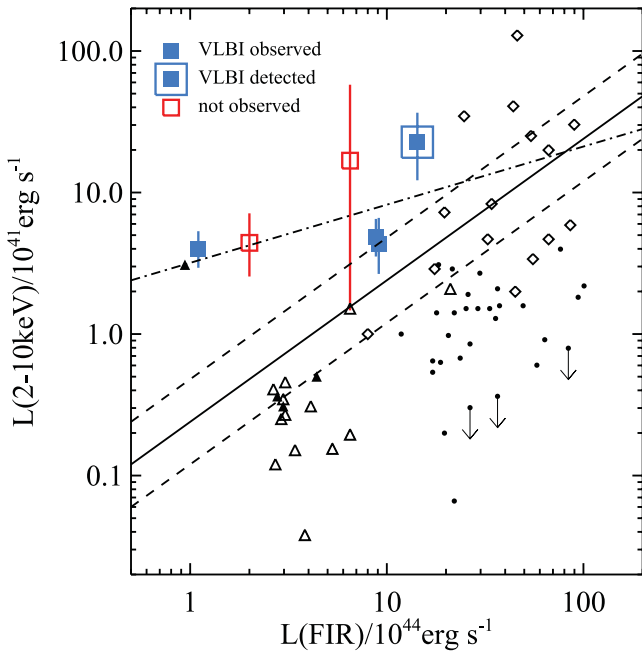


Figure 3. Hard X-ray luminosity versus far-infrared luminosity of LBAs from Jia et al. (2011), who observed six composite LBAs with *XMM-Newton*. The four composite LBAs also observed with VLBI are shown in blue, while the two composite LBAs not observed with VLBI are marked in red. The LBA composite J0921+4509 that was detected during our VLBI experiment is marked with a large blue square. Other samples shown for comparison are as follows: LIRGs and LIRG AGN from Lehmer et al. (2010) (open and filled triangles, respectively), LIRG AGN (diamonds) and hard X-ray quiet galaxies (small points) from Iwasawa et al. (2009). The solid line indicates the empirical $L_{X,2-10\text{keV}}-L_{\text{FIR}}$ relation from Ranalli, Comastri & Setti (2003), with the dashed lines showing an associated uncertainty of a factor of 2. The dash-dotted line is the best-fitting relation for the composite LBAs found by Jia et al. (2011).

the detection somewhat ambiguous. A stacked spectrum showed the potential detection of the 6.4 keV iron emission line (which is a key feature of obscured AGN), but only at the $\sim 2\sigma$ level. Jia et al. (2011) further found that the ratios of the mid-IR (24 μm) continuum to $[\text{O III}]\lambda 5007$ luminosities in these LBAs were higher than the values for typical Type 2 AGN by an average of 0.8 dex. Combining all these clues, it is likely that a hidden AGN is present in some or all of these composite LBAs, but that their bolometric luminosities are completely dominated by the intense starburst.

4.2 New insights from the VLBI data

The VLBI data on LBAs presented in this paper provide another piece of information on the issue of AGN in LBAs. As shown in Fig. 2, we have detected one out of the four composite LBAs observed with VLBI, and one out of the three H II-like LBAs. (Our third detection of a known AGN will not be discussed further here.)

On first sight, these results do not offer a clear dichotomy between star-forming and composite LBAs. Because all LBAs have extended radio structures due to star formation and SN activity extending to larger scales than those probed by VLBI (Basu-Zych et al. 2007), the emission we have detected could in principle be coming from certain compact, high surface brightness regions related to those structures. The fact that three of the four composite LBAs do not show any VLBI radio emission at all indicates that (1) the radio emission arising from their star-forming regions is completely resolved at milliarcsecond or parsec scales and (2) no (bright) radio AGN is present in these sources.

What other constraints do we have in order to study the relative contributions from starburst and AGN activity in this sample? Our detections have brightness temperatures of $\sim 10^5$ and $\sim 10^7$ K (see Table 3). These values are equal to (in the case of J0150+1308) and well in excess of (J0921+4509) the typical upper limit for thermal emission arising from star-forming regions ($\sim 10^5$ K), thus indicating that the emission in these objects is likely of non-thermal origin, at least in the case of J0921+4509 (Condon et al. 1991). Even though at these frequencies starburst emission may be dominated by non-thermal emission as well, their maximum brightness temperature still does not appear to exceed that limit. One interpretation is that the observed radio emission is associated with RSNe or SNRs. The non-detection at 5 GHz of both of our detections at 1.7 GHz supports this conclusion: our sources have steep spectra which may be indicative of RSNe or SNRs.

We can compare the total (non-thermal) radio luminosity detected from J0150+1308, $L_{1.7\text{GHz}} = 2.1 \times 10^{29} \text{ erg s}^{-1} \text{ Hz}^{-1}$, and J0921+4509, $L_{1.7\text{GHz}} = 1.4 \times 10^{29} \text{ erg s}^{-1} \text{ Hz}^{-1}$ (Table 4), with that expected based on nearby starburst galaxies for which it is possible to determine the relative contributions of individual RSNe and SNRs. The brightest RSNe observed in starburst galaxies have a

Table 4. Radio luminosity, physical size and resulting star formation rate for each of the 5σ detections. Should the radio emission be from a starburst the radio luminosity can be used to estimate the star formation rate. We calculated the SFR of our sources using the equation from Basu-Zych et al. (2007).

Source	$L_{1.7}$ ($10^{29} \text{ ergs s}^{-1} \text{ Hz}^{-1}$)	Physical size (pc)	SFR ($M_\odot \text{ yr}^{-1}$)
J0150+1308	2.116	146.2	7.78
J0921+4509	1.388	4.76	5.10
J1029+4829	1.540	<33.7	5.66

typical luminosity at 18 cm of the order of $2 \times 10^{27} \text{ erg s}^{-1} \text{ Hz}^{-1}$, while the most luminous RSNe ever observed (SN1988z) had $2 \times 10^{28} \text{ erg s}^{-1} \text{ Hz}^{-1}$ (Bondi et al. 2005). It is thus clear that the radio emission from LBAs requires large complexes of such SN (or an AGN). We will employ the well-studied examples of such complexes observed in the starburst galaxies Arp 299-A (Perez-Torres et al. 2009, 2010), Arp 220 (Lonsdale et al. 2006; Parra et al. 2007) and Mrk 273 (Bondi et al. 2005) to guide our discussion.

The central $150 \times 85 \text{ pc}$ region of Arp 299-A consists of a cluster of 26 RSNe and SNRs detected at 5 GHz, with a total luminosity coming from this region of $L_{5.0 \text{ GHz}} = 2 \times 10^{28} \text{ erg s}^{-1} \text{ Hz}^{-1}$, corresponding to $L_{1.7 \text{ GHz}} \approx 4.5 \times 10^{28} \text{ erg s}^{-1} \text{ Hz}^{-1}$ assuming a median spectral index of -0.72 for the region as a whole. The western nucleus of Arp 220 is another example of such a prolific SN factory: it consists of 18 individual RNSe/SNRs within a region of $50 \times 150 \text{ pc}$ and a total radio luminosity of $L_{1.7 \text{ GHz}} \approx 1.6 \times 10^{29} \text{ erg s}^{-1} \text{ Hz}^{-1}$.² In order to minimize potential systematic biases when we compare these objects with the LBAs, we will apply a scaling based on the ratios of the physical areas (A) observed and the total IR luminosities (L_{IR}) of these systems. The expected 18 cm luminosities for the LBAs are then $f_{\text{LBA}} * L_{\text{R}}$, where $f_{\text{LBA}} \approx (A_{\text{LBA}}/A_{\text{Arp220/Arp299-A}}) \times (L_{\text{IR,LBA}}/L_{\text{IR,Arp220/Arp299-A}})$ with $\log L_{\text{IR,Arp220}} = 12.27$ and $\log L_{\text{IR,Arp299-A}} = 11.53$. f_{LBA} was typically in the range of 1–2, and was never larger than a factor of 5, indicating that the comparison sample is well matched to the LBAs in terms of their SFRs and size of the physical regions probed. Next, we calculate the ratio of observed to expected radio luminosity for both LBAs.

For J0150+1308, the radio luminosity observed is, respectively, 1.7 and 2.8 times higher than that expected based on Arp 220 and Arp 299-A. For J0921+4509, and assuming that the source is resolved (see Section 3), the observed luminosity is, respectively, 2.9 and 4.8 times higher than that expected based on Arp 220 and Arp 299-A. If we assume that J0921+4509 is unresolved, its smaller area leads to observed luminosities that are higher than that expected by factors of 4.7 and 7.7. Similarly, if we compare with the brightest radio nucleus in Mrk 273, N1 with $L_{1.7 \text{ GHz}} \approx 7 \times 10^{28} \text{ erg s}^{-1} \text{ Hz}^{-1}$ (Bondi et al. 2005), the observed luminosities are again higher by factors of 2–3 for both LBAs. To summarize, our comparison shows that the radio luminosities of the LBAs are always higher than that expected by a factor of 2–3 for J0150+1308 and a factor of 3–8 for J0921+4509 suggesting that more than just star formation may be contributing to the radio emission observed.

4.3 The starburst interpretation

In Overzier et al. (2009) we argued that one explanation for the position in the BPT diagram of composite LBAs such as J0921+4509, together with their relatively low $L_{\text{H}\alpha}/L_{\text{FIR}}$, was that these are post-starbursts where the O stars were deficient and ionization by shocks (rather than photoionization by O stars) was very significant (our so-called ‘aged-starburst’ hypothesis, section 4.2.1 in that paper). However, confirmation of shock heating in the form of enhanced [S II] and [O I] line strengths was not found. New COS data on J0921+4509 imply a young age of $\sim 3 \text{ Myr}$ for the central starburst (Heckman et al. 2011; Borthakur et al., in preparation), ruling out

that model. These are young starbursts where the ionizing luminosity is at least an order-of-magnitude larger than the rate of kinetic energy supplied by SNe. While this does not mean that shocks may not be contributing (see Heckman et al. 2011 for evidence of high-velocity outflows), there is certainly no evidence for a weakness or an absence of ionizing radiation from stars that would lead to shock-dominated emission lines if this were an aged starburst. The starburst interpretation also fails to explain the excess X-ray emission observed in this source, unless an exotic starburst contribution to the hard X-ray emission is invoked (Jia et al. 2011).

4.4 The AGN interpretation

A more likely interpretation is that (some) composite LBAs host an AGN, consistent with the large excess compact radio emission observed on VLBI scales (in the case of J0921+4509). Unfortunately, we do not have sufficient resolution and sensitivity to look for further confirming evidence by resolving the core–jet structure in the radio, and the non-detections at 5 GHz imply that these low-luminosity sources may have significantly steeper spectra than those found in radio-loud AGN (e.g. Giroletti & Panessa 2009; Prandoni et al. 2010). On the other hand, there are now four independent indications that an AGN may be present: (1) the composite position in the BPT diagram, (2) the high VLBI luminosity, (3) the compact radio size, and (4) the hard X-ray excess found by Jia et al. (2011, see also Fig. 3). The offset into the AGN/composite region of the BPT diagram could then be the result of the strong ionizing radiation from the starburst with a small contribution from an obscured AGN (as well as some contribution from shocks).

If we assume that the VLBI detection in J0921+4509 is due to a radio AGN, we can compare it to typical radio-quiet quasars and Seyfert galaxies. Taking $L_{\text{X},2-10} = 2.3 \times 10^{42} \text{ erg s}^{-1}$ from Jia et al. (2011) and applying a factor of 2.86 to convert to $L_{\text{X},0.2-20}$ we find $L_{\text{R}}/L_{\text{X}} \approx 1.3 \times 10^{-4}$, about 10 times higher than that inferred from the $L_{\text{R}}/L_{\text{X}}$ relation from Laor & Behar (2008) who find $\langle L_{\text{R}}/L_{\text{X}} \rangle \sim 10^{-5}$ (with a 1σ scatter of about a factor 3 in L_{R}) for radio-quiet quasars. We compare this source to the BH ‘Fundamental Plane’ (FP) from Merloni, Heinz & di Matteo (2003, hereafter M03). Even though J0921+4509 was not detected at 5 GHz, we have extrapolated our 1.7 GHz detection to 5 GHz assuming a spectral index of -0.1 [consistent with the (5σ) upper limit for this source in the 5-GHz observation]. At face value, the result suggests a BH mass of a few $\times 10^7 M_{\odot}$. Much higher values are unlikely given the constraint on the radio luminosity, although there is significant uncertainty in the BH FP depending on the source of the radio and X-ray emission and the accretion state (see e.g. Plotkin et al. 2011). In a recent paper, de Gasperin et al. (2011) find that a sample of low-luminosity Type 2 AGN and low-ionization nuclear emission-line region (LINERS) do not lie on the BH FP of M03. Instead, based on their BH masses inferred from stellar velocity dispersions, the M03 relation would overpredict the M_{BH} of their sources by up to two orders of magnitude. In Jia et al. (2011) it was estimated that the candidate Type 2 AGN in the composite LBAs may have BH masses in the range of 10^5 – $10^6 M_{\odot}$ if these objects are radiating at the Eddington limit, but they could be higher for sub-Eddington BHs. On the other hand, Overzier et al. (2009) showed that the central mass concentration on a scale of $\sim 100 \text{ pc}$ is consistent with a ‘protobulge’ of the order of $10^9 M_{\odot}$ in stars. Assuming a standard bulge–BH mass scaling relation, it is hard to imagine the presence of a BH substantially more massive than $\sim 10^7 M_{\odot}$. The presence of a compact radio core has at least made it convincingly clear that

² It should be noted that Downes & Eckart (2007) found evidence for a weak AGN in the western nucleus of Arp 220. If this is the case then the radio excess we detect would either be the result of many additional RNSe/SNRs, though that would be unlikely, or the result of a stronger AGN.

an AGN is present in J0921+4509, but it is impossible to give better constraints on the BH mass than 10^5 – $10^7 M_{\odot}$.

We can compare the results from our small sample with the results of Parra et al. (2010) who analysed the radio AGN fraction among a much larger sample of relatively nearby, ‘warm’ IR luminous galaxies (wLIRGs) across the BPT diagram, also using VLBI. In some respects, their sample can be considered to be the more obscured equivalent of our UV-selected LBA sample (see Overzier et al. 2009). The wLIRGs and LBAs are shown in Fig. 2 (small dots), where sources with large circles indicate VLBI detections. While most of the wLIRG sources with optical spectra indicative of a dominant AGN were detected in VLBI, most (~ 80 per cent) of the sources in the AGN–starburst composite region of the diagram were, in fact, not (see also Corbett et al. 2003). This situation is similar to the non-detections for three of our four composite LBAs. One may naively expect that the chance of detecting an AGN increases significantly as one moves from pure H II-like objects to pure AGN-like objects across the BPT diagram, contrary to what is observed. One explanation for the lack of VLBI detections among the composite LBAs and wLIRGs could be that the high gas columns of the dense nuclear gas associated with the starbursts lead to significant free–free absorption, which would especially affect these composite systems. In this case, it would be better to observe at higher frequencies in order to offset the λ^2 dependence of the free–free opacity, although we note that we did not detect anything at 5.0 GHz either (including the known 1.7 GHz source J0921+4509). On the other hand, even with a relatively high L_R/L_X of 10^{-4} as found for J0921+4509, the remaining composite LBA sources would have been hard to detect given their hard X-ray luminosities (about a factor of 10 lower). Not only are the radio AGN expected to be intrinsically faint, the relatively high redshift of our sources ($z \sim 0.2$) complicates their detectability with VLBI. Alternatively, given AGN variability as observed in some LLAGN (Bell et al. 2011), or the episodic accretion expected in some cosmological galaxy formation models (e.g. Hopkins & Quataert 2010), it is perhaps not surprising that our very small sample observed produced only one clear detection of an accreting BH in the radio as the X-ray observations were performed at a different epoch.

5 SUMMARY AND FUTURE PROSPECTS

This paper presents the results of a pilot program to observe LBAs with composite spectra intermediate between pure starbursts and Type 2 AGN for comparison with objects whose optical emission line ratios did not appear to suggest the presence of an obscured AGN. The VLBI data obtained with the EVN were combined with data previously obtained in the X-ray from *XMM-Newton*, optical from Sloan Digital Sky Survey (SDSS) and mid-IR and far-IR (FIR) from *Spitzer* to further constrain the nature of these objects that are of special interest given their demonstrated similarities to galaxies that were common only at high redshift. While it might be expected that composite objects are detected more frequently than pure H II-like regions only ~ 20 per cent of our composite LBAs were detected, possibly due to free–free absorption.

Three sources, J0150+1308, J0921+4509 and J1029+4829 were detected above 5σ , and all had brightness temperatures close to or in excess of the typical upper limit for thermal emission from star-forming regions. In addition, J0150+1308 and J0921+4509 had radio luminosities two to eight times above that expected from multiple RSNs and SNRs in the starbursts Arp 220, Arp 229A and Mrk 273 after a careful normalization based on the different resolutions and total SFRs.

In particular, the composite LBA J0921+4509 displayed a compact core, most likely unresolved as confirmed by Monte Carlo simulation, emitting around 10 per cent of observed VLA flux. The source also possessed an excess L_R expected from the L_R/L_X ratio of radio-quiet AGN, while its L_X was found to be high relative to the value expected based on its SFR (Jia et al. 2011). This suggests a source of radio and X-ray emission beyond that expected of a pure starburst. We conclude therefore that this excess is most probably due to an obscured AGN with an estimated BH mass of $\sim 10^5$ – $10^7 M_{\odot}$.

As stated in Section 1, one of our main motivations for probing BH formation in these LBAs as local analogues of LBGs is the question of whether the young starburst-dominated galaxies seen at high redshift already carry the ‘seeds’ of supermassive BHs detected in the local universe. If so, these small-to-moderate mass BHs at high redshift may reveal their presence through AGN activity. It is currently not clear whether BHs would be able to accrete very efficiently in these young and dense starburst-dominated regions, or whether a delay should exist between the onset of a central starburst and the accretion on to the central BH (e.g. Norman & Scoville 1988; Davies et al. 2007). Taken together, our X-ray and radio results shown here indicate that LLAGN can co-exist in young, dense starbursts, but our sample is currently too small to put strong constraints on this timing argument.

It is important to point out that at radio wavelengths, the contribution of these AGN is still only a fraction of the total radio flux density, making the identification of such sources based on radio data practically impossible much beyond $z \sim 0.2$ (see below). Even in the X-rays, the combined luminosity from SFR and candidate AGN in LBAs (Jia et al. 2011, fig. 3) is lower or comparable to that detected in the deepest X-ray stacks of star-forming galaxies at $z \sim 3$ – 4 (Laird et al. 2006; Zheng et al. 2010), illustrating that individual detections are likely out of reach for current X-ray observatories. Also discussed in this paper, the interpretation of optical emission-line diagnostic diagrams for identifying weak AGN is not trivial either, especially in the case of shocks or due to the limited physical resolution achieved in high-redshift data (see fig. 12 in Overzier et al. 2009, for a large compilation of BPT information from low- and high-redshift galaxies). These limitations indicate the important role that nearby galaxies still play in studying the AGN–starburst (or BH–host galaxy) connection.

Our pilot program of searching for AGN in the most extreme UV-selected starbursts in the relatively nearby universe demonstrates the unique power of VLBI to assess the prevalence of accreting BHs and SN complexes in young, star-forming galaxies. With this goal in mind, we conclude with investigating the prospects for future VLBI detection experiments. In Fig. 4 we show the predicted 1.4 GHz flux densities for (weak) radio AGN as a function of redshift up to $z = 1$. The blue, green and red shaded areas show the 1.4 GHz flux densities expected for a compact core having L_R/L_X ratios of 10^{-5} (i.e. typical radio-quiet AGN), 10^{-4} (i.e. that measured for the LBA composite J0921+4509) and 10^{-3} . The upper boundary of each region assumes $L_X \sim 5 \times 10^{42} \text{ erg s}^{-1}$ (i.e. comparable to that of J0921+4509), while the lower boundaries are for sources that are a factor of 10 less luminous in the X-ray (i.e. comparable to the other composite LBAs studied in this paper). Horizontal lines indicate typical EVN 5σ sensitivities achieved in a 1-h (dotted line) and 4-h observation (solid line) both at 1 Gbps recording, as well as the projected 4-h sensitivity expected in the next few years (dashed line). A source similar to J0921+4509 both in L_X and L_R/L_X can be detected to a redshift of $z \sim 0.4$, while it could be seen out to $z \sim 0.8$ if its radio loudness (L_R/L_X) was 10 times higher. In contrast,

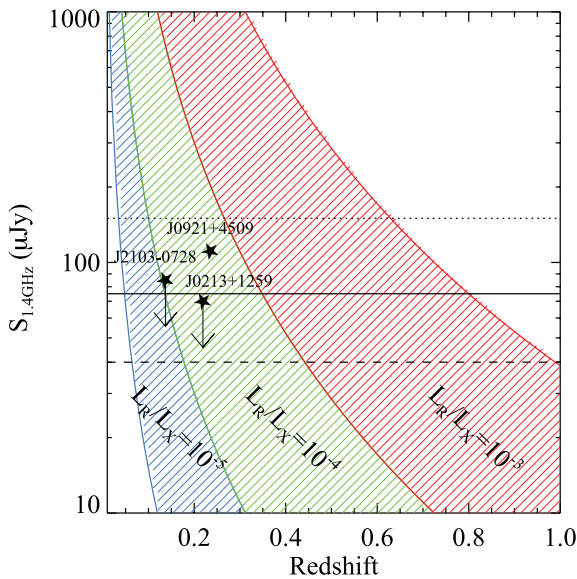


Figure 4. Predicted flux densities for low-luminosity radio AGN as a function of redshift. The blue, green and red shaded areas show the 1.4 GHz flux densities expected for a compact core having L_R/L_X ratios of 10^{-5} (i.e. typical radio-quiet AGN), 10^{-4} (i.e. $10\times$ more luminous), and 10^{-3} (i.e. $100\times$ more luminous). The upper boundary of each region assumes $L_X \sim 5 \times 10^{42} \text{ erg s}^{-1}$ (i.e. comparable to that of J0921+4509), while the lower boundaries are for sources that are a factor 10 less luminous in the X-rays (i.e. comparable to the other composite LBAs studied in this paper). Our detection of the probable AGN in J0921+4509 is indicated by the star, while two undetected composite LBAs are shown as upper limits. Horizontal lines indicate typical EVN 5σ sensitivities achieved in a 1-h (dotted line) and 4-h observation (solid line) both at 1 Gbps recording, as well as the projected 4-h sensitivity of the EVN with new telescopes becoming available in the next few years (dashed line).

the prospects for sources that are radio quiet and a factor of 10 less luminous in the X-ray are grim: such sources could potentially be detected only out to $z \sim 0.1$.

The recently increased sky coverage in the UV (*GALEX*), optical (SDSS) and IR (*WISE*) will allow the efficient selection of exotic starbursts, composites and AGN at relatively low redshifts suitable for VLBI. A systematic survey of their pc-scale radio emission offers a unique chance of gaining new insights into the complex nuclear processes occurring in galaxies over a very wide redshift range.

ACKNOWLEDGMENTS

The EVN is a joint facility of European, Chinese, South African and other radio astronomy institutes funded by their national research councils. We thank Patricia Arévalo, Jenny Greene, Lisa Kewley and Miguel Pérez Torres for discussions. We would also like to thank the referee for his or her helpful feedback.

REFERENCES

Adelberger K. L., Steidel C. C., Pettini M., Shapley A. E., Reddy N. A., Erb D. K., 2005, *ApJ*, 619, 697
 Alexander D. M., Bauer F. E., Chapman S. C., Smail I., Blain A. W., Brandt W. N., Ivison R. J., 2005, *ApJ*, 632, 736
 Baldwin J. A., Phillips M. M., Terlevich R., 1981, *PASP*, 93, 5
 Basu-Zych A. R. et al., 2007, *ApJS*, 173, 457

Basu-Zych A. et al., 2009, *ApJ*, 699, L118
 Bell M. E. et al., 2011, *MNRAS*, 411, 402
 Biggs A. D., Younger J. D., Ivison R. J., 2010, *MNRAS*, 408, 342
 Bondi M., Pérez-Torres M.-A., Dallacasa D., Muxlow T. W. B., 2005, *MNRAS*, 361, 748
 Condon J. J., Huang Z. P., Yin G. F., Thuan T. X., 1991, *ApJ*, 378, 65
 Corbett E. A. et al., 2003, *ApJ*, 583, 670
 Davies R. I., Sánchez F. M., Genzel R., Tacconi L. J., Hicks E. K. S., Friedrich S., Sternberg A., 2007, *ApJ*, 671, 1388
 de Gasperin F., Merloni A., Sell P., Best P., Heinz S., Kauffmann G., 2011, *MNRAS*, 415, 2910
 Di Matteo T., Springel V., Hernquist L., 2005, *Nat*, 433, 604
 Diamond P. J., 1995, in Zensus J. A., Diamond P. J., Napier P. J., eds, *ASP Conf. Ser. Vol. 82, Very Long Baseline Interferometry and the VLBA*. Astron. Soc. Pac., San Francisco, p. 227
 Downes D., Eckart A., 2007, *A&A*, 468, L57
 Elmegreen B. G., Bournaud F., Elmegreen D. M., 2008, *ApJ*, 684, 829
 Gallimore J. F., Axon D. J., O’Dea C. P., Baum S. A., Pedlar A., 2006, *AJ*, 132, 546
 Gebhardt K. et al., 2000, *ApJ*, 539, L13
 Giroletti M., Panessa F., 2009, *ApJ*, 706, L260
 Gonçalves T. S. et al., 2010, *ApJ*, 724, 1373
 Heckman T. M. et al., 2005a, *ApJ*, 619, L35
 Heckman T. M., Ptak A., Hornschemeier A., Kauffmann G., 2005b, *ApJ*, 634, 161
 Heckman T. M. et al., 2011, *ApJ*, 730, 5
 Hoopes C. G. et al., 2007, *ApJS*, 173, 441
 Hopkins P. F., Quataert E., 2010, *MNRAS*, 407, 1529
 Iwasawa K., Sanders D. B., Evans A. S., Mazzarella J. M., Armus L., Surace J. A., 2009, *ApJ*, 695, L103
 Jia J., Ptak A., Heckman T. M., Overzier R. A., Hornschemeier A., LaMassa S. M., 2011, *ApJ*, 731, 55
 Kauffmann G. et al., 2003, *MNRAS*, 346, 1055
 Kettenis M., van Langevelde H. J., Reynolds C., Cotton B., 2006, in Gabriel C., Arviset C., Ponz D., Solano E., eds, *ASP Conf. Ser. Vol. 351, Astronomical Data Analysis Software and Systems XV*. Astron. Soc. Pac., San Francisco, p. 497
 Kewley L. J., Heisler C. A., Dopita M. A., Sutherland R., 2000, *ApJ*, 530, 704
 Kewley L. J., Groves B., Kauffmann G., Heckman T., 2006, *MNRAS*, 372, 961
 Kimball A. E., Kellermann K. I., Condon J. J., Ivezić Ž., Perley R. A., 2011, *ApJ*, 739, L29
 Laird E. S., Nandra K., Hobbs A., Steidel C. C., 2006, *MNRAS*, 373, 217
 Laor A., Behar E., 2008, *MNRAS*, 390, 847
 Lehmer B. D. et al., 2005, *AJ*, 129, 1
 Lehmer B. D., Alexander D. M., Bauer F. E., Brandt W. N., Goulding A. D., Jenkins L. P., Ptak A., Roberts T. P., 2010, *ApJ*, 724, 559
 Lonsdale C. J., Diamond P. J., Thrall H., Smith H. E., Lonsdale C. J., 2006, *ApJ*, 647, 185
 Magorrian J. et al., 1998, *AJ*, 115, 2285
 Merloni A., Heinz S., di Matteo T., 2003, *MNRAS*, 345, 1057 (M03)
 Norman C., Scoville N., 1988, *ApJ*, 332, 124
 Ouchi M. et al., 2008, *ApJS*, 176, 301
 Overzier R. A. et al., 2008, *ApJ*, 677, 37
 Overzier R. A. et al., 2009, *ApJ*, 706, 203
 Overzier R. A., Heckman T. M., Schiminovich D., Basu-Zych A., Gonçalves T., Martin D. C., Rich R. M., 2010, *ApJ*, 710, 979
 Overzier R. A. et al., 2011, *ApJ*, 726, L7
 Padovani P., Miller N., Kellermann K. I., Mainieri V., Rosati P., Tozzi P., 2011, *ApJ*, 740, 20
 Parra R., Conway J. E., Diamond P. J., Thrall H., Lonsdale C. J., Lonsdale C. J., Smith H. E., 2007, *ApJ*, 659, 314
 Parra R., Conway J. E., Aalto S., Appleton P. N., Norris R. P., Pihlström Y. M., Kewley L. J., 2010, *ApJ*, 720, 555
 Pérez-Torres M. A., Romero-Canizales C. M. A., Alberdi A., Polatidis A., 2009, *A&A*, 507, L17

- Perez-Torres M. A., Alberdi A., Romero-Canizales C., Bondi M., 2010, *A&A*, 519, L5
- Plotkin R. M., Markoff S., Kelly B. C., Koerding E., Anderson S. F., 2011, preprint (arXiv:1105.3211)
- Prandoni I., de Ruiter H. R., Parma P., Gregorini L., Ekers R. D., 2010, *A&A*, 510, 42
- Ranalli P., Comastri A., Setti G., 2003, *A&A*, 399, 39
- Rich J. A., Kewley L. J., Dopita M. A., 2011, *ApJ*, 734, 87
- Shepherd M. C., Pearson T. J., Taylor G. B., 1994, *BAAS*, 26, 987
- Steidel C. C., Hunt M. P., Shapley A. E., Adelberger K. L., Pettini M., Dickinson M., Giavalisco M., 2002, *ApJ*, 576, 653
- Yuan T.-T., Kewley L. J., Sanders D. B., 2010, *ApJ*, 709, 884
- Zheng Z. Y., Wang J. X., Finkelstein S. L., Malhotra S., Rhoads J. E., Finkelstein K. D., 2010, *ApJ*, 718, 52

This paper has been typeset from a $\text{\TeX}/\text{\LaTeX}$ file prepared by the author.